DCE-MRI Analysis Methods for Predicting the Response of Breast Cancer to Neoadjuvant Chemotherapy: Pilot Study Findings

Xia Li,[1] Lori R. Arlinghaus,[1] Gregory D. Ayers,[2] A. Bapsi Chakravarthy,[3,4]
Richard G. Abramson,[1,4,5] Vandana G. Abramson,[4,6] Nkiruka Atuegwu,[1,5] Jaime Farley,[4]
Ingrid A. Mayer,[6] Mark C. Kelley,[4,7] Ingrid M. Meszoely,[4,7] Julie Means-Powell,[4,6]
Ana M. Grau,[4,7] Melinda Sanders,[4,8] Sandeep R. Bhave,[9]
and Thomas E. Yankeelov[1,4,5,10,11,12]*

Purpose: The purpose of this pilot study is to determine (1) if early changes in both semiquantitative and quantitative DCE-MRI parameters, observed after the first cycle of neoadjuvant chemotherapy in breast cancer patients, show significant difference between responders and nonresponders and (2) if these parameters can be used as a prognostic indicator of the eventual response.
Methods: Twenty-eight patients were examined using DCE-MRI pre-, post-one cycle, and just prior to surgery. The semiquantitative parameters included longest dimension, tumor volume, initial area under the curve, and signal enhancement ratio related parameters, while quantitative parameters included K^{trans}, v_e, k_{ep}, v_p, and τ_i estimated using the standard Tofts-Kety, extended Tofts-Kety, and fast exchange regime models.

Results: Our preliminary results indicated that the signal enhancement ratio washout volume and k_{ep} were significantly different between pathologic complete responders from non-responders ($P < 0.05$) after a single cycle of chemotherapy. Receiver operator characteristic analysis showed that the AUC of the signal enhancement ratio washout volume was 0.75, and the AUCs of k_{ep} estimated by three models were 0.78, 0.76, and 0.73, respectively.
Conclusion: In summary, the signal enhancement ratio washout volume and k_{ep} appear to predict breast cancer response after one cycle of neoadjuvant chemotherapy. This observation should be confirmed with additional prospective studies. **Magn Reson Med 00:000–000, 2013. © 2013 Wiley Periodicals, Inc.**

Key words: DCE-MRI; breast cancer; neoadjuvant therapy; treatment response

[1]Vanderbilt University Institute of Imaging Science (VUIIS), Vanderbilt University, Nashville, Tennessee, USA.

[2]Department of Biostatistics, Vanderbilt University, Nashville, Tennessee, USA.

[3]Department of Radiation Oncology, Vanderbilt University, Nashville, Tennessee, USA.

[4]Vanderbilt Ingram Cancer Center, Vanderbilt University, Nashville, Tennessee, USA.

[5]Department of Radiology and Radiological Sciences, Vanderbilt University, Nashville, Tennessee, USA.

[6]Department of Medical Oncology, Vanderbilt University, Nashville, Tennessee, USA.

[7]Department of Surgical Oncology, Vanderbilt University, Nashville, Tennessee, USA.

[8]Department of Pathology, Vanderbilt University, Nashville, Tennessee, USA.

[9]School of Medicine, Washington University in St. Louis, Missouri, USA.

[10]Department of Physics and Astronomy, Vanderbilt University, Nashville, Tennessee, USA.

[11]Department of Biomedical Engineering, Vanderbilt University, Nashville, Tennessee, USA.

[12]Department of Cancer Biology, Washington University in St. Louis, Missouri, USA.

*Correspondence to: Thomas E. Yankeelov, Ph.D., Vanderbilt University Institute of Imaging Science, Vanderbilt University Medical Center, AA-1105 Medical Center North, 1161 21st Avenue South, Nashville, Tennessee 37232-2310. E-mail: thomas.yankeelov@vanderbilt.edu

Dynamic contrast enhanced magnetic resonance imaging (DCE-MRI) involves the serial acquisition of heavily T_1-weighted MR images of a tissue of interest (e.g., a tumor) before and after an intravenous injection of paramagnetic contrast agent (CA). As the CA enters into a tissue, it changes the measured MR signal intensity to a degree that depends on its local distribution and concentration. When the CA is transported out of the tissue the MR signal intensity returns to its baseline value. By analyzing the associated signal intensity time course using an appropriate pharmacokinetic model, physiological parameters related to, for example, blood flow, vessel permeability, and tissue volume fractions can be extracted for each image voxel or region of interest (1).

There have been many efforts employing DCE-MRI as a surrogate biomarker for assessing and predicting the response of breast tumors to neoadjuvant chemotherapy. Early studies focused on semiquantitative analyses employing changes in tumor volume as measured by contrast enhanced MRI to evaluate treatment response (2–4). For example, Cheung et al. (2) analyzed tumor size differences between pre-treatment and after one cycle of chemotherapy, and final tumor size response on 33 patients and found all complete responders (defined as patients without residual cancer) had a tumor size reduction of >45% after one cycle of therapy. Chou et al. (3) segmented the tumor volumes of all enhancing voxels

before and after neoadjuvant chemotherapy on 17 breast cancer patients. They reported that the segmented voxels displaying fast and steady state washout characteristics was highly correlated with the histopathologic estimation of viable neoplastic tissue volume after therapy. Martincich et al. (4) also noted the tumor volume reduction after two cycles of chemotherapy was associated with a major histopathological response, based on the analysis of 30 patients. For other examples of using morphology and anatomical measures to assess response, the interested reader is referred to references (5–8).

Although the above results are encouraging, morphological characteristics (such as tumor size and qualitative enhancement patterns) are the temporally downstream effects of underlying physiological changes, so it is reasonable to hypothesize that changes in metrics of, for example, tumor perfusion could serve as a surrogate biomarker of early response to treatment. Therefore, in addition to assessing changes in tumor size, investigators have begun to examine the quantitative physiological parameters available from DCE-MRI. Indeed, some efforts have shown that quantitative analysis of DCE-MRI data can accurately assess (9) or predict treatment response (10,11), as well as predict 5-year survival (12–16). Padhani et al. (10) performed DCE-MRI examinations in 25 patients with primary breast cancer and found both tumor size and change in the range of the volume transfer constant (i.e., K^{trans}) on the histogram after two cycles of treatment were equally able to predict eventual response. Ah-See et al. (11) acquired DCE-MRI data on 28 patients with primary breast cancer and, by calculating the changes in seven pharmacokinetic parameters, they reported that change in the volume transfer constant (K^{trans}) was the best predictor of pathologic nonresponse. However, not all studies have shown that quantitative DCE-MRI yields results superior to that obtained by simple volumetrics. For example, Yu et al. (17) reported that changes in early tumor size as estimated from enhancing voxels after one cycle of neoadjuvant chemotherapy led to a higher area under the receiver operating characteristic (ROC) curve than pharmacokinetic parameters estimated in DCE-MRI. We return to this point in the Discussion section.

Thus, while there have been efforts to employ quantitative analysis of DCE-MRI to predict therapy response in breast cancer patients receiving neoadjuvant chemotherapy, the field has not yet determined which techniques and analysis methods—or the time of application of those methods—are optimal. Considering the significant differences in tumor type, treatment regimen, number of patients, clinical and pathological endpoints, as well as imaging data acquisition and modeling techniques, it is not surprising that there is currently a lack of consensus on this issue. In this study, we contribute to the developing literature on using DCE-MRI to predict the response of breast cancer to neoadjuvant chemotherapy by investigating the predictive ability of seven semiquantitative and 11 quantitative pharmacokinetic parameters returned from three DCE-MRI pharmacokinetic models. The purpose of this pilot study is to determine if early changes in both semiquantitative and quantitative DCE-MRI parameters, observed after the first cycle of neoadjuvant chemotherapy, show significant differences between responders and nonresponders, and if these parameters can be used as prognostic indicators of the eventual response. To the best of our knowledge, this is the first effort to perform such an analysis in this patient population.

METHODS

Patient Selection

Patients undergoing neoadjuvant chemotherapy as a component of their clinical care were eligible to participate in the study. No prior systemic therapies for breast cancer were allowed. All patients had histologically documented invasive carcinoma of the breast with a sufficient risk of recurrence, based on pretreatment clinical parameters of size, grade, age, and nodal status, to warrant the use of chemotherapy at the discretion of their treating medical oncologist. Participating patients provided informed written consent to our Institutional Review Board approved study.

Treatment Schema

The neoadjuvant chemotherapy regimen was left to the discretion of the treating oncologist based on patient factors such as menopausal status and age as well as tumor characteristics such as size, grade, nodal status, and receptor status. Receptor testing, including estrogen, progesterone, and HER2/neu receptor testing, can be used to identify breast tumor molecular subtype and therefore guide treatment regimens. ER and PR assays were considered positive if there were at least 1% positive tumor nuclei in the sample on testing in the presence of expected reactivity of internal (normal epithelial elements) and external controls (18). A positive HER2 result was IHC staining of 3+ (uniform, intense membrane staining of >30% of invasive tumor cells), a fluorescent in situ hybridization result of more than six HER2 gene copies per nucleus or a fluorescent in situ hybridization ratio (HER2 gene signals to chromosome 17 signals) of more than 2.2; a negative result was an IHC staining of 0 or 1+, a fluorescent in situ hybridization result of <4.0 HER2 gene copies per nucleus, or fluorescent in situ hybridization ratio of <1.8. Equivocal results required additional action for final determination (19). Table 1 lists the receptor status for all patients and the corresponding treatment regimens. DCE-MRI was performed at baseline (after diagnosis but before the initiation of chemotherapy, t_1), after one cycle (t_2), and at the completion of all therapy just prior to surgery (t_3).

Study Design

Thirty-six female patients with stage II/III breast cancer were enrolled in this prospective study (in which patient recruitment is ongoing). Eight patients were not included in these analyses due to the following reasons: withdrawal from the study after the first scan ($n = 6$), hardware failure on the scanner ($n = 1$), and issues with the contrast line ($n = 1$). Thus, 28 patients were available for assessing the ability of the semiquantitative and quantitative DCE-MRI metrics to predict treatment response, while 22 patients were available for comparing the longest dimensions (LDs) of the tumor as measured by

Table 1
Clinical Features of the Study Population

Patient #	Age (yr)	Treatment Regimens	Receptor status (ER, PR, and HER2)	Size Pretreatment (cm)	Tumor grade	Residual tumor size (cm)	Pathologic response
1	50	AC → taxol	+, +, −	10	3	0.52	Nonresponder
2	52	Taxotere	+, −, +	5	3	1.5	Nonresponder
3	60	AC → taxol + concurrent traztuzumab	+, +, +	5	2	2.9	Nonresponder
4	36	Taxol + Cisplatin ± Everolimus	−, −, −	7	2	2.9	Nonresponder
5	48	Dose-dense AC → Taxol	+, +, −	3	1	1.3	Nonresponder
6	43	Dose-dense AC → Taxol	+, +, −	6	2	2.6	Nonresponder
7	59	Dose-dense AC → Taxol	+, +, −	7	2	4.2	Nonresponder
8	53	Taxol + Cisplatin ± Everolimus	−, −, −	3.5	2	1.3	Nonresponder
9	35	Trastuzumab + Carboplatin + Ixabepilone	+, +, +	4	3	1.4	Nonresponder
10	28	Taxol + Cisplatin ± Everolimus	−, −, −	2	3	0.8	Nonresponder
11	33	AC → taxol	+, +, −	5	3	1.2	Nonresponder
12	39	AC → taxol	+, +, −	10	1	2.5	Nonresponder
13	57	AC → taxol	−, +, +	5.5	3	n/a	Nonresponder
14	67	Dose-dense AC → Taxol	−, +, +	8	3	1.2	Nonresponder
15	45	Taxol + Cisplatin ± Everolimus	−, −, −	3	3	0.5	Nonresponder
16	46	Taxotere + carboplatin + herceptin	+, +, +	7	3	0.3	Nonresponder
17[a]	47	Taxotere → AC	+, +, −	6	1	0	Nonresponder
18	53	AC → concurrent Taxol + trastuzumab	−, −, +	4	3	0	Responder
19	46	Taxotere → AC	−, +, −	5	3	0	Responder
20	46	AC → concurrent Taxol + trastuzumab	−, −, +	12	2	0	Responder
21	33	AC → weekly taxol	−, −, −	10	3	0	Responder
22	39	Trastuzumab and Lapatinib	−, −, +	3.5	2	0	Responder
23	46	AC → taxol	+, −, −	2	3	0	Responder
24	42	Taxol + Cisplatin ± Everolimus	−, −, −	3	3	0	Responder
25	34	Taxotere → AC	−, −, −	3	3	0	Responder
26	44	Trastuzumab + Lepatinib	−, −, +	6	3	0	Responder
27	37	Taxol + Cisplatin ± Everolimus	−, −, −	4.5	3	0	Responder
28	39	AC → taxol	−, −, −	2.5	3	0	Responder

[a]No residual tumor was found in the breast for this patient; however, the cancer was found in 6 lymph nodes.

surgical pathology to the third MRI exam obtained after completion of neoadjuvant chemotherapy and just prior to surgery. The median age of the patients was 45 years old (range, 28–67 years). The median time between t_1 and t_2 was 14 days (range, 5–28 days) and the median time between t_2 and t_3 was 109 days (range, 57–209 days).

Table 1 summarizes the salient features of the study population including the pretherapy tumor sizes as measured by physical exam. The post therapy tumor size was determined from the surgical specimen, and 11 patients were defined as pathologic complete responders (pCRs; i.e., complete absence of tumor in the surgical specimen), while 17 patients were defined as nonresponders (non-pCRs).

MRI Data Acquisition

DCE-MRI was performed using a Philips 3T Achieva MR scanner (Philips Healthcare, Best, The Netherlands). A 4-channel receive double-breast coil covering both breasts was used for 20 patients (Invivo, Gainesville, FL), while a 16-channel double-breast coil was used for eight patients. Data for constructing a T_1 map were acquired with an RF-spoiled 3D gradient echo multi-flip angle approach with TR = 7.9 ms, TE = 1.3 ms, and 10 flip angles from 2 to 20 degrees in two degree increments. The acquisition matrix was $192 \times 192 \times 20$ (full-breast) over a sagittal square field of view (22×22 cm^2) with

slice thickness of 5 mm, one signal acquisition, and a SENSE factor of 2 for an acquisition time of just under 3 min. The dynamic scans used identical parameters and a flip angle of 20°. Each 20-slice set was collected in 16 s at 25 time points for ∼7 min of scanning. For the DCE study, a catheter placed within an antecubital vein delivered 0.1 mmol/kg (9 − 15 mL, depending on patient weight) of the CA gadopentetate dimeglumine, Gd-DTPA, (Magnevist, Wayne, NJ) at 2 mL/s (followed by a saline flush) via a power injector (Medrad, Warrendale, PA) after the acquisition of three baseline dynamic scans.

Data Analysis

Determination of the Enhancement Threshold

In an attempt to limit user intervention (i.e., to maximally automate the post-processing steps), we sought to determine a rational enhancement threshold that could be automatically applied to all DCE-MRI data prior to performing data analysis. We elected to choose the enhancement threshold that resulted in the highest agreement between the DCE-MRI tumor LD at t_3 with the tumor size measured by surgical pathology. Using such an enhancement threshold would provide a reasonable estimate of actual tumor voxels to include for the semi-quantitative and quantitative analyses. Toward this end, for each patient at each time point, the whole tumor

volume was conservatively segmented by manually drawing an region of interest to completely surround the enhancing tumor as seen on each tumor slice. Given this initial set of voxels, subsets of tumor voxels were constructed on the basis of their percent enhancement which was defined as $\left((\bar{S}_{post} - \bar{S}_{pre})/\bar{S}_{pre}\right) \cdot 100$, where $\bar{S}_{post}$ is the averaged post-contrast signal intensity and $\bar{S}_{pre}$ is the average of the three pre-contrast time points. A total of 20 subsets were defined for percent enhancement thresholds ranging from 10 to 200% in 10% increments. We then computed the concordance correlation coefficient [the CCC measures the absolute agreement between two variables; (20)] between the LD of the tumor measured on the surgical specimen and the LD measured on the DCE-MRI data at t_3. As the largest CCC (0.74) was obtained with an enhancing threshold of 80%, all subsequent analysis were based on voxels that showed $\geq 80\%$ enhancement.

Semiquantitative Analysis

Seven parameters in the semiquantitative analysis were estimated: tumor volume, the LD, the initial area under the curve at 60 s (iAUC$_{60}$), the signal enhancement ratio (SER), SER total tumor volume, SER partial volume, and SER washout volume (21). SER was calculated according to reference (21):

$$SER = \frac{S_1 - S_0}{S_2 - S_0}, \qquad [1]$$

where S_1 was the peak signal, S_0 was the mean precontrast signal (first to third dynamic scans), and S_2 was the signal at the 25th dynamic scan. The SER total tumor volume was defined as the number of all enhancing voxels. The SER partial volume was the number of voxels with SER ≥ 0.9, and the SER washout volume was the number of voxels with SER > 1.3 (21).

Quantitative analysis

Three pharmacokinetic models were used to estimate physiological parameters from the DCE-MRI data. The standard Tofts-Kety model (TK) assumes a linear relationship between the time-varying longitudinal relaxation time, $T_1(t)$, and the concentration of CA in the tissue, $C_t(t)$:

$$R_1(t) \equiv 1/T_1(t) = r_1 C_t(t) + R_{10}, \qquad [2]$$

where R_{10} is the R_1 value of the tissue before CA administration, and r_1 is the relaxivity of the CA. The C_t time course together with the concentration of CA in the blood (the arterial input function, C_p, or AIF; see below) can then be input to the TK model to estimate the volume transfer constant (K^{trans}, min^{-1}) and the extravascular extracellular volume fraction (v_e):

$$C_t(T) = K^{trans} \cdot \int_0^T C_p(t) \cdot e^{-(K^{trans}/v_e)\cdot(T-t)} dt. \qquad [3]$$

The extended Tofts-Kety model (ETK) makes similar assumptions as the TK, but incorporates the plasma volume fraction (v_p):

$$C_t(T) = K^{trans} \int_0^T C_p(t) \exp\left(-(K^{trans}/v_e)(T-t)\right) dt + v_p C_p(t). \qquad [4]$$

The third model used in the study is the fast exchange regime model (FXR). Rather than assuming that all water compartments within tissue are well mixed, as in the TK and ETK models, the FXR model assumes that tissue is compartmentalized on the scale of an MRI voxel (22–24). The FXR model incorporates the effects of water exchange between the extravascular-extracellular space and the extravascular intracellular space, leading to a nonlinear relationship between $T_1(t)$ and $C_t(t)$:

$$
\begin{aligned}
R(t) = 1/T_1(t) = {} & \frac{1}{2}\left(2R_{1i} + r_1 C_t(t) + \frac{(R_{10} - R_{1i} + 1/\tau_i)}{(v_e/f_w)}\right) \\
& + \frac{1}{2}\left(\left(\frac{2}{\tau_i} - r_1 C_t(t) - \frac{R_{10} - R_{1i} + 1/\tau_i}{v_e f_w}\right)^2 \right. \\
& \left. + 4\frac{(1 - v_e/f_w)}{\tau_i^2(v_e/f_w)}\right)^{1/2},
\end{aligned}
$$
$$[5]$$

where R_{1i} is the intracellular R_1, τ_i is the average intracellular water lifetime of a water molecule, and f_w is the fraction of water that is accessible to mobile CA (22,25,26), which is set to 1.0 in this study. In this realization, the FXR returns estimates of K^{trans}, v_e, and τ_i (22,25–28). All three models also estimate efflux constant, k_{ep} ($\equiv K^{trans}/v_e$, min^{-1}).

The three DCE-MRI pharmacokinetic models were applied to all tumor voxels that displayed an enhancement percentage $\geq 80\%$ to estimate K^{trans}, k_{ep}, and v_e (all three models), v_p (ETK only), and τ_i (FXR only). Those parameters were estimated by a standard gradient-expansion, nonlinear, least-squares, and curve-fitting algorithm written in the Interactive Data Language (Research Systems, Boulder, CO). Voxels for which the fitting algorithm did not converge, or converged to nonphysical values (i.e., $K^{trans} > 5.0$ min^{-1}, $v_e > 1.0$, or any parameter below 0.0) were set equal to zero and not included in subsequent analysis.

As mentioned above, in order to perform quantitative DCE-MRI, the AIF must be measured. Individual AIFs were not available for each patient at each time point and, therefore, a population based AIF is a reasonable approach. We employed a semiautomatic AIF tracking algorithm to obtain individual AIFs in 50 datasets. These 50 AIFs were then used to construct a population-averaged AIF, which was then used for subsequent DCE-MRI modeling. Details on this procedure can be found in Ref. (29).

Statistical Analysis

There are two main steps in the statistical analysis: (1) identifying which parameters show significant differences after one cycle of therapy between (eventual)

Table 2

Median (Interquartile Range) Percent Change in the Semiquantitative Parameters from t_1 to t_2

Parameter (% change from t_1 to t_2)	Responders (%)	Nonresponders (%)	P value[a]
Volume	−34.0 (−57.33 to −22.34)	−28.7 (−51.81 to −4.93)	0.37
LD	−22.6 (−37.31 to −8.62)	−8.6 (−27.63 to 10.34)	0.26
iAUC$_{60}$	−20 (−41 to 17)	−3 (−14 to 27)	0.32
SER	−15 (−21.5 to −10.5)	−3.0 (−17 to 4)	0.14
SER total	−34 (−57 to −22)	−29 (−52 to 4)	0.40
SER partial	−56 (−70.5 to −30)	−43 (−63 to 6)	0.37
SER Washout	−80 (−91.5 to −71)	−55 (−79 to −24)	0.03[b]

[a]Wilcoxon rank sums test.
[b]FDR adjusted P-value $= 0.18$.

responders and nonresponders and (2) in the parameters that do show a significant difference between the two patient sets, determine their prognostic ability by performing ROC analysis.

Percent changes in the mean value of the region of interest for each parameter from t_1 to t_2 were summarized using the median and interquartile range. Due to graphical evidence of non-normality, we used the nonparametric Wilcoxon rank sums test to compare the distribution of these data between the two response groups (30). Comparisons were considered statistically significant (i.e., rejection of the null hypothesis of equality) for P-value < 0.05. While the P-value is a quantity associated with a single hypothesis test, it is also important to assess the expected number of false discoveries among many individually statistically significant ($P < 0.05$) tests (31). Among the 18 statistical comparisons, we calculated the false discovery rate (FDR) adjusted P-values (i.e., q-values) for statistically significant results. We consider FDR adjusted P-values < 0.2 to be true discoveries, accepting that one in five positive findings will be false discoveries.

ROC curves were estimated for predicting responders for each parameter (32). The optimal cut-point for each parameter satisfies the Youden index, the point on the ROC curve, which is furthest from chance and minimizes the overall rate of misclassification (33). The AUC was estimated using the trapezoidal rule and 95% confidence intervals for the AUC's were estimated using the nonparametric bootstrap method (with 10,000 replicates). Using similar bootstrap methods, the AUC was compared between imaging metrics (with 10,000 replicates). The number of replicates was chosen to establish reliable estimates to two significant digits. Data were analyzed using MATLAB R2012a (The Mathworks, Natick, MA) and the pROC library built under R version 2.15 (34).

RESULTS

Neither the baseline semiquantitative nor the quantitative parameters differed significantly between eventual responders and nonresponders. Table 2 shows the median percent changes and interquartile range of the semiquantitative parameters for both nonresponders and responders. Amongst the semiquantitative parameters, only the change in SER washout volume showed a significant difference between responder and nonresponder patients ($P = 0.03$).

Figure 1 displays representative data of a patient achieving pathologic complete response acquired at the three time points (three columns) in the form of the average of the post contrast MR images (top row), the difference images between the precontrast and postcontrast DCE-MRI data (middle row), and K^{trans} values superimposed on the averaged post-contrast DCE-MRI data (bottom row), respectively; Figure 2 displays similar data for one nonresponder. For both patients, the tumor areas are clearly enhanced at t_1 and t_2 (left and middle columns). For the complete responder, and the mean values of K^{trans} at t_1 and t_2 estimated by TK were 0.21 and 0.19 min^{-1}, respectively, while there was no enhancing tumor after all cycles of treatment (right column). For the nonresponder patient, the enhancing tumors were evident in all three MRI scans and the mean values of K^{trans} at three time points estimated by TK were 0.20, 0.24, and 0.16 min^{-1}, respectively.

Figure 3 provides an example of the early changes in pharmacokinetic parameters estimated by the TK, ETK, and FXR models. The median changes of k_{ep} estimated by all three models were significantly different between responders and nonresponders. The other parameters showed no statistically significant differences between groups. These data are summarized in Table 3, which presents the median percent changes and interquartile range of the quantitative parameters for the three DCE-MRI models included in the study.

Table 4 summarizes the results of the ROC analysis for the most promising semiquantitative and quantitative parameters: the SER washout volume and k_{ep}. The table lists the optimal cutoff, sensitivity, specificity, and the AUC. The TK model estimate of k_{ep} resulted in the largest AUC value of 0.78, compared with 0.76 and 0.73, obtained by the ETK and FXR models, respectively. There was not a statistical difference between the AUCs of the SER washout volume and k_{ep} as estimated by any of the three models ($P > 0.50$ in all comparisons.). The 95% confidence interval was also calculated for the ROC values. Lower limits for the AUCs that exclude 0.5 indicate the accuracy of the parameters exceeds what would be expected by chance alone. Following a Bonferroni correction, the bootstrapped lower limits of the AUCs for SER washout and k_{ep} estimated by the TK, ETK, and FXR models were 0.52, 0.57, 0.53, and 0.49, respectively. Hence, all parameters excepts for k_{ep} estimated by the FXR model retained statistical significance. Figure 4 shows the ROC curves for the SER washout volume and k_{ep} estimated by three models. The AUC values and the optimal cutoff points are also displayed in the figure.
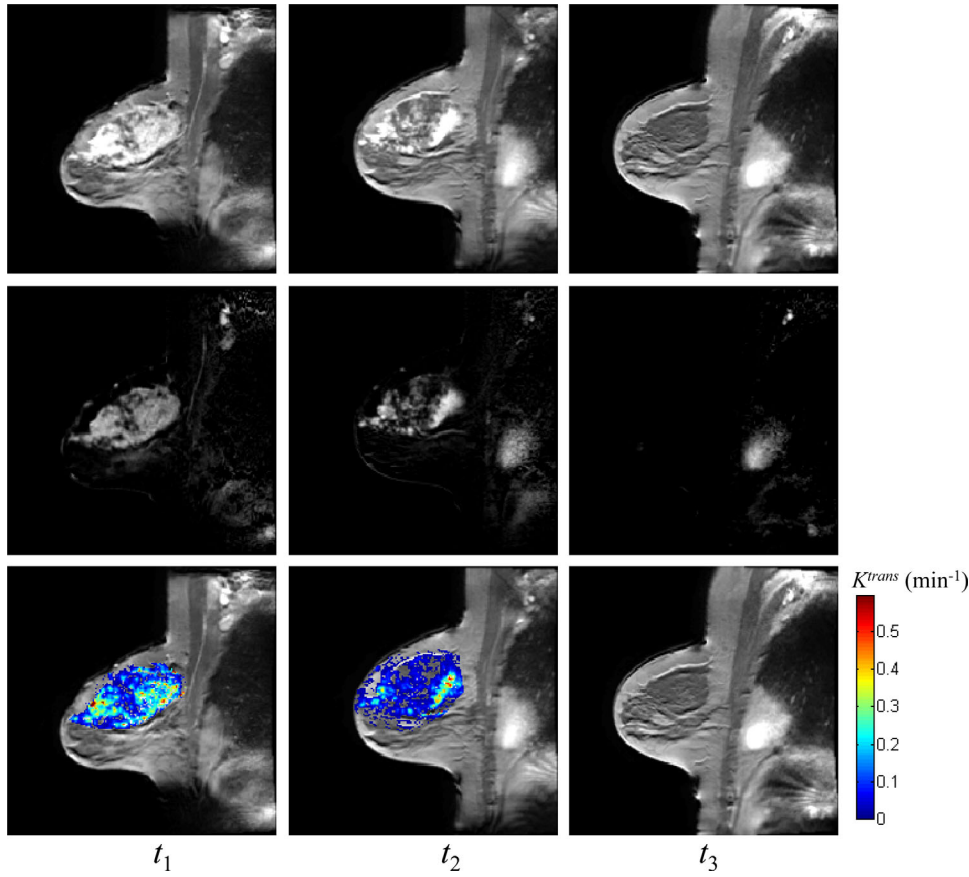
FIG. 1. The averaged post-contrast MR images (top row), the difference images between pre-contrast and postcontrast DCE data (middle row), and K^{trans} values superimposed on the averaged postcontrast images (bottom row) at three time points (three columns) for one pathological complete responder. The mean values of K^{trans} at three time points estimated by TK are 0.21, 0.19, and 0 min^{-1}, respectively, using 80% enhancement threshold.
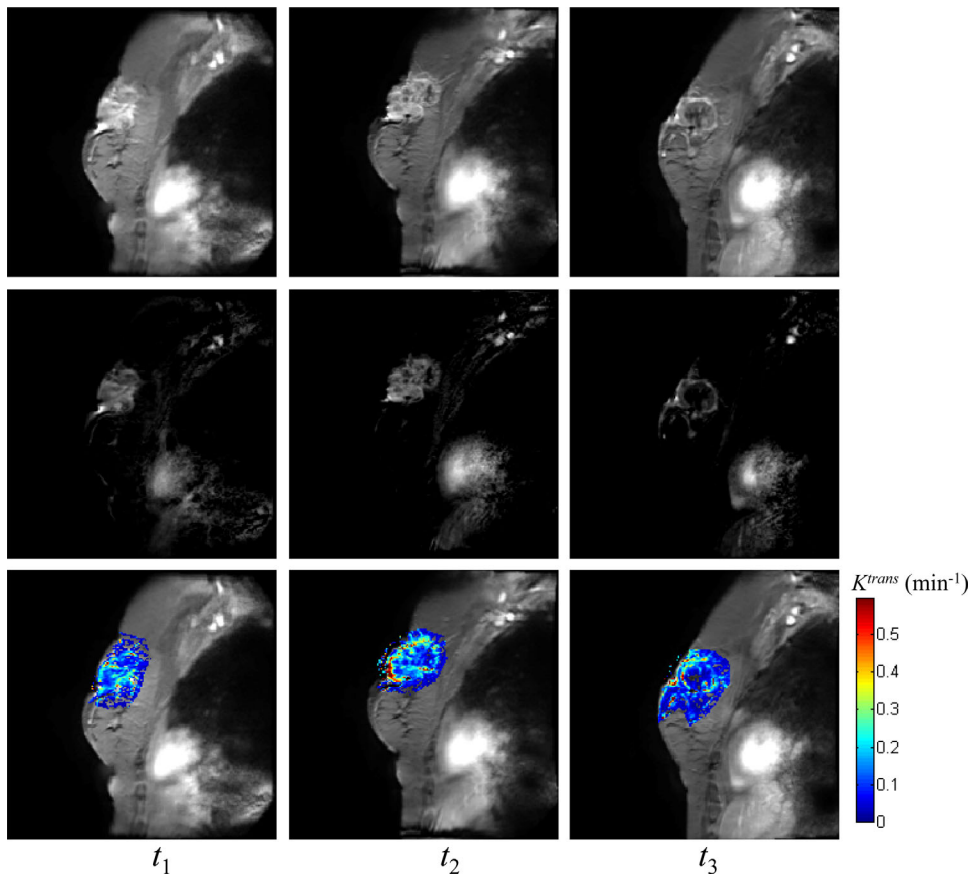

FIG. 2. The averaged postcontrast MR images (top row), the difference images between pre-contrast and postcontrast DCE data (middle row), and K^{trans} values superimposed on the averaged postcontrast data (bottom row) at three time points (three columns) for one nonresponder. The mean values of K^{trans} at three time points estimated by TK are 0.20, 0.24, and 0.16 min^{-1}, respectively, using a 80% enhancement threshold.
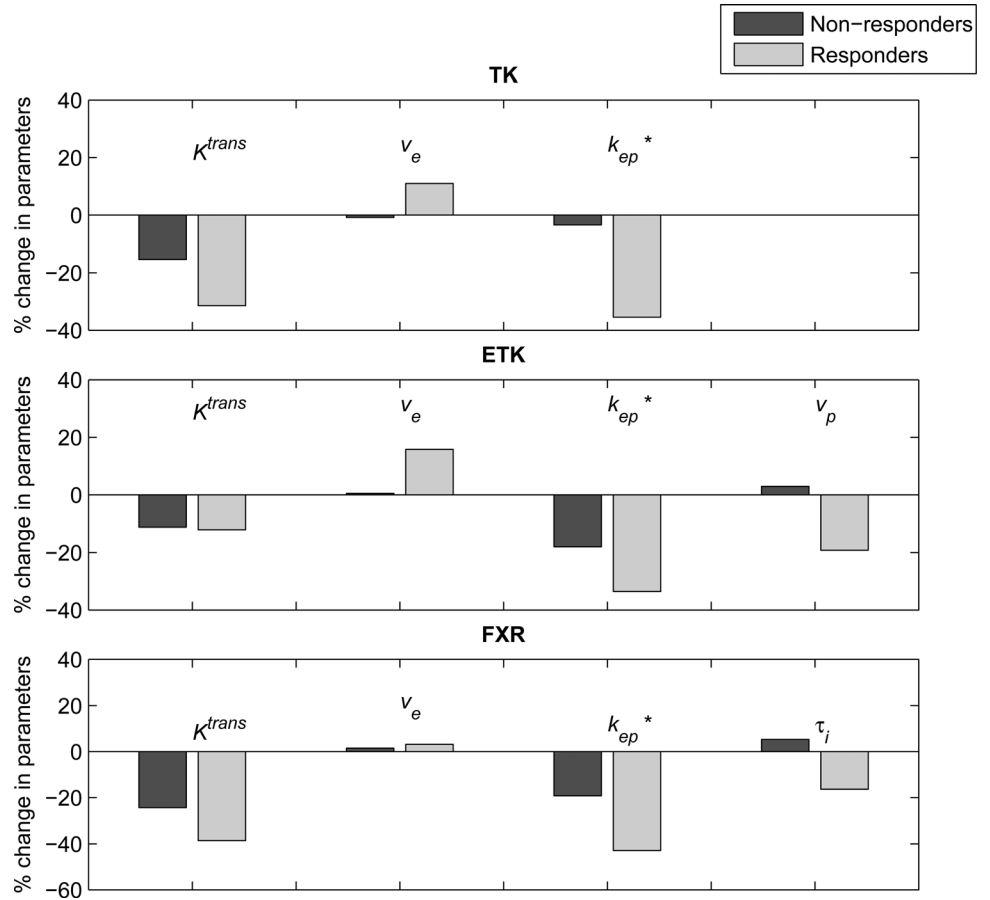
FIG. 3. The median changes in kinetic parameters estimated by the TK, ETK, and FXR models. All statistically significant differences ($P < 0.05$) are labeled with an asterisk.

Among the 18 comparisons, four statistically significant ($P < 0.05$) discoveries were made. A FDR of 20% (FDR adjusted P-value < 0.2) implies that we expect one false discovery among five individually significant comparisons. The FDR adjusted P-values for SER washout volume and k_{ep} estimated by the TK and ETK models were all 0.18 (Tables 2 and 3). The FDR adjusted P-value for k_{ep} estimated by FXR was 0.22 (Table 3). Consequently, we can conclude that differences in the distributions of SER washout volume and k_{ep} estimated by the TK and ETK models between complete responders and nonresponders retain statistical significance after adjusting for a FDR of 20%. Despite the likelihood that k_{ep} estimated by FXR may be a false discovery, we still assessed its ROC characteristics for completeness since k_{ep} retained significance in the other two models.

DISCUSSION

This study presents a comparison of the ability of a range of common semiquantitative and quantitative DCE-MRI parameters obtained pre- and post-one cycle of neoadjuvant chemotherapy to predict treatment response. The semiquantitative parameters were obtained through

Table 3

Median (Interquartile Range) Percent Changes of the Quantitative Parameters from t_1 to t_2 for the Three DCE-MRI Models

DCE-MRI model	Parameter (% change from t_1 to t_2)	Responders (%)	Nonresponders (%)	P value
TK	K^{trans}	−31 (−35.5 to −11.5)	−15 (−30 to 25)	0.13
	v_e	11 (−4.5 to 19)	−1 (−13 to 12)	0.37
	k_{ep} (=K^{trans}/v_e)	−35 (−49.5 to −26)	−3 (−31 to 13)	0.01[a]
ETK	K^{trans}	−12 (−25 to −2.5)	−11 (−29 to 16)	0.54
	v_p	−19 (−34.5 to −0.5)	3 (−24 to 77)	0.26
	v_e	16 (−3.5 to 20)	0 (−12 to 18)	0.26
	k_{ep} (=K^{trans}/v_e)	−34 (−40.5 to −27)	−18 (−37 to −16)	0.02[a]
FXR	K^{trans}	−39 (−57 to −23.5)	−24 (−47 to 33)	0.17
	v_e	3 (0 to 8)	1 (−7 to 5)	0.26
	τ_i	−16 (−24 to 1)	5 (−23 to 18)	0.26
	k_{ep} (=K^{trans}/v_e)	−43 (−58 to −23.5)	−19 (−36 to −2)	0.048[b]

[a]FDR adjusted P-value = 0.18.
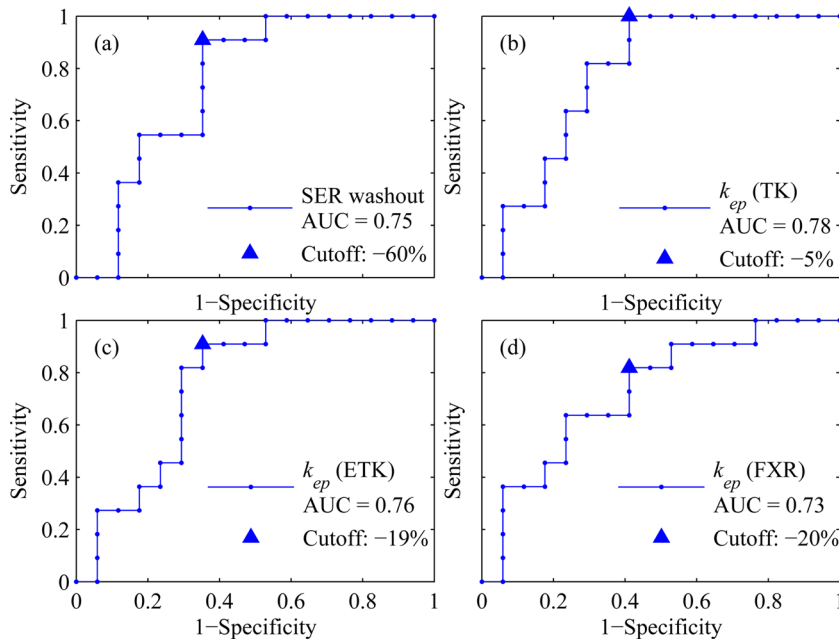[b]FDR adjusted P-value = 0.22.

FIG. 4. The ROC curves for (panel a) the SER washout volume and k_{ep} estimated by (b) the TK, (c) ETK, and (d) FXR models. The triangle represents the optimal cutoff points as determined by the Youden index.

calculating the LD and volume of the breast tumors, as well as dynamic parameters related to the area under the enhancement curve and the SER. The quantitative analysis explored each parameter returned by the TK, ETK, and FXR models. Although previous studies (9–11,17,35) have examined the ability of dynamic MRI to assess the response of breast cancer patients to neoadjuvant chemotherapy, to the best of our knowledge ours is the first to investigate the most frequently used semiquantitative metrics and quantitative DCE-MRI parameters estimated by different models.

Overall, the results indicate that changes in k_{ep} from t_1 to t_2, as estimated by the TK and ETK models, were significantly different between eventual responders and nonresponders after a single cycle of chemotherapy. We hypothesize the following biological basis for this observation. As k_{ep} is the efflux rate constant, it attempts to quantify the degree to which a signal intensity time course exhibits washout characteristics. If k_{ep} is large, it means that there is a combination of relatively high delivery (i.e., high blood flow and/or vessel permeability) and a relatively small extravascular extracellular space for the CA to accumulate. The former can be attributed to tumor associated vasculature, while the latter can be attributed to an increased (tumor) cell density in such a section of tissue. Consequently, the concentration of CA in the

vascular and extravascular space will equilibrate rapidly. Then, once the concentration of CA in the vascular space falls below the concentration in the extracascular space, the CA will then intravasate back into the vascular space and this phenomenon manifests itself as a high k_{ep}. Thus, in this setting (i.e., predicting the response of breast cancer to neoadjuvant therapy) a reduction in k_{ep} could be associated with positive response as it is most likely associated with a reduction in delivery and/or cellularity. Furthermore, the SER washout volume, which attempts to characterize this phenomenon in a semiquantitative fashion, is also able to separate the two patient groups. We also note that both k_{ep} and the SER washout attempt to quantity (to varying degrees) so-called "type III" washout kinetics, which has been widely used in the diagnostic setting (36) to assist in the identification of malignant lesions. In light of these observations, we feel k_{ep} is a promising biomarker for response.

It is important to note that ours are not the first data to indicate that k_{ep} may outperform K^{trans} and v_e when examining longitudinal changes in breast cancer during neoadjuvant therapy. In particular, several previous efforts (17,37,38) all showed that k_{ep} had the greatest ability of the DCE-MRI parameters to separate responders from nonresponders. Unfortunately, the underlying physiological reason that k_{ep} potentially outperforms other

Table 4
ROC Analysis of Percent Change in SER Washout and k_{ep} for Predicting Treatment Response

Parameter	Optimal Cutoff (%)	Sensitivity (%) 95% CI	Specificity (%) 95% CI	AUC[a] (95% CI)
%SER_washout	−60	91 (62 − 99)	65 (41 − 83)	0.75[b] (0.55 − 0.91)
%k_{ep}, TK	−5	100 (74 − 100)	59 (36 − 78)	0.78[b] (0.60 − 0.94)
%k_{ep}, ETK	−19	91 (62 − 99)	65 (41 − 83)	0.76[b] (0.57 − 0.92)
%k_{ep}, FXR	−20	82 (52 − 95)	59 (36 − 78)	0.73 (0.55 − 0.91)

The 95% confidence intervals (CI) were also calculated for sensitivity, specificity, and AUC.
[a]Lower limits for AUC that exclude 0.5 indicate the accuracy of the parameter exceeds what would be expected by chance alone.
[b]These parameters retain statistical significance following a Bonferroni correction that protects the overall type I error inference for AUC at 5%.

DCE-MRI parameters has not been fully determined and this study was not intended to address this important issue. Future studies should be designed to elucidate the underlying mechanism of this observation.

Our previous study (27) assessed the three pharmacokinetic models statistically and found the ETK and FXR models were superior to the TK model at describing the DCE-MRI data. However, the results in this study showed that the TK and ETK models gave superior results in their ability to statistically significantly separate patient groups (e.g., see Table 4). A likely reason for this is that since the ETK and FXR models have a third free parameter (v_p and τ_i for the ETK and FXR, respectively), the parameters that are returned necessarily have greater uncertainty. Thus, it is possible that these models require DCE-MRI data with a higher signal-to-noise ratio to achieve the same level of precision in estimated parameters as the TK model. This decrease in parameter precision would potentially manifest itself as a decreased ability to separate patient groups. It is entirely possible that higher signal-to-noise ratio data would increase the predictive value of the ETK and FXR. The possibility should also not be overlooked, however, that the additional parameters included in the ETK and FXR models may have only limited biological relevance in this setting.

It is important to interpret the present data in light of the recently published results of the ACRIN 6657/I-SPY TRIAL (39) in which 216 women with invasive breast cancers $\geq$ 3 cm (our study accepts tumors down to 1 cm in size) were scanned by a high spatial resolution (and, therefore, low temporal resolution) DCE-MRI protocol at four time points: prior to the start of anthracycline-cyclophosphamide chemotherapy, prior to the second cycle of anthracycline-cyclophosphamide chemotherapy, between anthracycline-cyclophosphamide treatment and taxane therapy, and just prior to surgery. The investigators assessed the ability of four variables to predict treatment response: the SER (21,40), peak SER, tumor LD, and tumor volume. Among other results, this study showed the rate of change of the tumor volume and the SER between therapeutic regimens were the most predictive of pathologic complete response with area under the receiver operator curves of 0.72 and 0.71, respectively. Thus, a semiquantitative metric (i.e., the SER) based on high spatial resolution data performed nearly as well as tumor volume changes. It is entirely possible, therefore, that a more quantitative analysis of higher temporal resolution DCE-MRI data could achieve even more significant results. The results of this study seem to indicate this is a reasonable hypothesis.

There are a number of limitations in the study. First, a population AIF was used to estimate physiological parameters from the DCE-MRI data. In practice, it is difficult to obtain a reliable AIF from each patient at each scanning session, so a population based AIF is an alternative approach. As a previous study (29) indicated that K^{trans} and v_p show a good agreement between the population AIF and individual AIF, the population AIF was employed in this analysis. A possible future analysis is to compare the results returned when individual AIFs are employed in the DCE-MRI analysis.

A second limitation to consider is that the temporal resolution of 16 s is, admittedly, not optimal for AIF characterization; rather it represents a balance between temporal resolution, spatial resolution, and field of view coverage. The central issue is that we needed to be able to cover the entire breast because our study was also designed to analyze changes at the voxel level after longitudinal registration (41,42). This requirement necessitated an increase in slice number to cover the entire affected breast, which led to a longer *TR* and, therefore, a longer acquisition time. Hence, the current acquisition represents a practical implementation of the approach and the results are encouraging. Furthermore, since our study employed a population AIF that had previously been tested (29), the 16 second temporal resolution is quite reasonable for sampling and subsequently estimating tissue pharmacokinetic parameters (43). We note that some studies (11,44,45) have employed only modestly faster temporal resolutions with success; in particular, the study by Ah-See et al. (11) in breast cancer employed a temporal resolution of 12 s, which was sufficient to show that changes in DCE-MRI can predict final clinical and pathologic response.

A third limitation is using pathologic response as an outcome measure. Although survival is ultimately the endpoint of greatest interest in cancer clinical trials and as a general rule response must not be equated with survival outcomes, pathologic complete response as an outcome measure in the setting of neoadjuvant chemotherapy for breast cancer is valuable. For example, Wolff et al. (46) discussed pathologic complete response as a prognostic marker for overall survival, as established first in the NSABP (National Surgical Adjuvant Breast and Bowel Project) B-18 trial (47) and later confirmed in the NSABP B-27 trial (48). The authors concluded that while pathologic complete response was not a perfect replacement for survival, it was useful from a statistical viewpoint, and as such it has become the primary endpoint in most if not all trials of neoadjuvant therapy in breast cancer.

The final limitation is that our patient population received a number of different treatment regimens (see Table 1). However, there is currently disagreement in the (limited) literature over the effect this has on the ability of MRI to predict response in the neoadjuvant setting. For example, Loo et al. (49) showed in a population of 188 women that MRI is quite accurate when monitoring response in triple-negative and HER2+ disease, but is not in ER+/HER2- disease. Conversely, De Los Santos et al. (50), in a study of 81 patients, indicated that molecular subtype and systemic therapy did not significantly affect the ability of MRI to predict pathologic response. As both of these articles were very recent additions to the literature, it appears this is an important area for further study.

Our preliminary results indicate that changes in the SER washout volume and k_{ep} appear significantly different between eventual responders and nonresponders in breast cancer patients after the first cycle of neoadjuvant chemotherapy. These two approaches also yielded reasonable and promising AUC values. Future work includes performing ROC analysis through combining

the most predictive DCE-MRI parameters with DW-MRI data [also obtained in this ongoing study, (51)] to evaluate the feasibility of using quantitative MRI data to predict the response of breast cancers to neoadjuvant chemotherapy at this early stage. Another future aim is to investigate the tumor heterogeneity contained in parametric maps. Padhani et al. (10) examined the changes in K^{trans} range (similar to the standard deviation metric used in this study) and were able to predict the absence of pathologic response after two cycles of chemotherapy. O'Connor et al. (52) also showed that DCE-MRI biomarkers of tumor heterogeneity may predict colorectal cancer liver metastasis shrinkage. Hence, we hypothesize that the spatial distribution of pharmacokinetic parameters is important and that longitudinal registration of such data may improve the ability of DCE-MRI data to predict treatment response (41,42,53). Longer term, we plan to perform a follow-up analysis to compare the DCE-MRI results to progression free survival and 5 year survival.

In summary, this work, combined with related reports in the literature (2–11,17,35), may ultimately allow clinicians to use serial functional imaging rather than anatomic measurements as a more precise way to determine response to therapeutic agents, and thereby tailor therapy on an individual basis for this patient population. Given the multiple experimental measurements performed in this work, the findings of this pilot study should be followed up with a prospective study designed to confirm our data regarding the likely importance of k_{ep} in predicting treatment response.

ACKNOWLEDGMENTS

REFERENCES

1. Yankeelov TE, Gore JC. Dynamic contrast enhanced magnetic resonance imaging in oncology: Theory, data acquisition, analysis, and examples. Curr Med Imaging Rev 2007;3:91–107.

2. Cheung YC, Chen SC, Su MY, See LC, Hsueh S, Chang HK, Lin YC, Tsai CS. Monitoring the size and response of locally advanced breast cancers to neoadjuvant chemotherapy (weekly paclitaxel and epirubicin) with serial enhanced MRI. Breast Cancer Res Treat 2003;78: 51–58.

3. Chou CP, Wu MT, Chang HT, Lo YS, Pan HB, Degani H, Furman-Haran E. Monitoring breast cancer response to neoadjuvant systemic chemotherapy using parametric contrast-enhanced MRI: A pilot study. Acad Radiol 2007;14:561–573.

4. Martincich L, Montemurro F, De Rosa G, et al. Monitoring response to primary chemotherapy in breast cancer using dynamic contrast-enhanced magnetic resonance imaging. Breast Cancer Res Treat 2004; 83:67–76.

5. Wasser K, Klein SK, Fink C, Junkermann H, Sinn HP, Zuna I, Knopp MV, Delorme S. Evaluation of neoadjuvant chemotherapeutic response of breast cancer using dynamic MRI with high temporal resolution. Eur Radiol 2003;13:80–87.

6. Drew PJ, Kerin MJ, Mahapatra T, Malone C, Monson JR, Turnbull LW, Fox JN. Evaluation of response to neoadjuvant chemoradiotherapy for locally advanced breast cancer with dynamic contrast-enhanced MRI of the breast. Eur J Surg Oncol 2001;27:617–620.

7. Abraham DC, Jones RC, Jones SE, et al. Evaluation of neoadjuvant chemotherapeutic response of locally advanced breast cancer by magnetic resonance imaging. Cancer 1996;78:91–100.

8. Gilles R, Guinebretiere JM, Toussaint C, et al. Locally advanced breast cancer: contrast-enhanced subtraction MR imaging of response to preoperative chemotherapy. Radiology 1994;191:633–638.

9. Yankeelov TE, Lepage M, Chakravarthy A, et al. Integration of quantitative DCE-MRI and ADC mapping to monitor treatment response in human breast cancer: initial results. Magn Reson Imaging 2007;25: 1–13.

10. Padhani AR, Hayes C, Assersohn L, Powles T, Makris A, Suckling J, Leach MO, Husband JE. Prediction of clinicopathologic response of breast cancer to primary chemotherapy at contrast-enhanced MR imaging: initial clinical results. Radiology 2006;239:361–374.

11. Ah-See ML, Makris A, Taylor NJ, et al. Early changes in functional dynamic magnetic resonance imaging predict for pathologic response to neoadjuvant chemotherapy in primary breast cancer. Clin Cancer Res 2008;14:6580–6589.

12. Pickles MD, Manton DJ, Lowry M, Turnbull LW. Prognostic value of pre-treatment DCE-MRI parameters in predicting disease free and overall survival for breast cancer patients undergoing neoadjuvant chemotherapy. Eur J Radiol 2009;71:498–505.

13. Heldahl MG, Bathen TF, Rydland J, Kvistad KA, Lundgren S, Gribbestad IS, Goa PE. Prognostic value of pretreatment dynamic contrast-enhanced MR imaging in breast cancer patients receiving neoadjuvant chemotherapy: overall survival predicted from combined time course and volume analysis. Acta Radiol 2010;51:604–612.

14. Johansen R, Jensen LR, Rydland J, Goa PE, Kvistad KA, Bathen TF, Axelson DE, Lundgren S, Gribbestad IS. Predicting survival and early clinical response to primary chemotherapy for patients with locally advanced breast cancer using DCE-MRI. J Magn Reson Imaging 2009; 29:1300–1307.

15. Newitt DC, Partridge SC, Chang B, Joe BN, Hylton N. Optimization of the percent enhancement threshold for breast MRI tumor volume measurement during neoadjuvant treatment of breast cancer for predicting recurrence free survival time. In Proceedings of the 19th Annual Meeting of ISMRM, Montreal, Canada, 2011. p. 208.

16. Li SP, Makris A, Beresford MJ, et al. Use of dynamic contrast-enhanced MR imaging to predict survival in patients with primary breast cancer undergoing neoadjuvant chemotherapy. Radiology 2011;260:68–78.

17. Yu HJ, Chen JH, Mehta RS, Nalcioglu O, Su MY. MRI measurements of tumor size and pharmacokinetic parameters as early predictors of response in breast cancer patients undergoing neoadjuvant anthracycline chemotherapy. J Magn Reson Imaging 2007;26:615–623.

18. Hammond ME, Hayes DF, Dowsett M, et al. American Society of Clinical Oncology/College Of American Pathologists guideline recommendations for immunohistochemical testing of estrogen and progesterone receptors in breast cancer. J Clin Oncol 2010;28:2784–2795.

19. Wolff AC, Hammond ME, Schwartz JN, et al. American Society of Clinical Oncology/College of American Pathologists guideline recommendations for human epidermal growth factor receptor 2 testing in breast cancer. J Clin Oncol 2007;25:118–145.

20. Lin LI. A concordance correlation coefficient to evaluate reproducibility. Biometrics 1989;45:255–268.

21. Arasu VA, Chen RC, Newitt DN, Chang CB, Tso H, Hylton NM, Joe BN. Can signal enhancement ratio (SER) reduce the number of recommended biopsies without affecting cancer yield in occult MRI-detected lesions? Acad Radiol 2011;18:716–721.

22. Yankeelov TE, Rooney WD, Li X, Springer CS. Variation of the relaxographic "shutter-speed" for transcytolemmal water exchange affects the CR bolus-tracking curve shape. Magnet Reson Med 2003; 50:1151–1169.

23. Yankeelov TE, Rooney WD, Huang W, Dyke JP, Li X, Tudorica A, Lee JH, Koutcher JA, Springer CS Jr. Evidence for shutter-speed variation in CR bolus-tracking studies of human pathology. NMR Biomed 2005; 18:173–185.

24. Li X, Huang W, Yankeelov TE, Tudorica A, Rooney WD, Springer CS Jr. Shutter-speed analysis of contrast reagent bolus-tracking data: preliminary observations in benign and malignant breast disease. Magn Reson Med 2005;53:724–729.

25. Landis CS, Li X, Telang FW, et al. Determination of the MRI contrast agent concentration time course in vivo following bolus injection: effect of equilibrium transcytolemmal water exchange. Magnet Reson Med 2000;44:563–574.

26. Zhou R, Pickup S, Yankeelov TE, Springer CS Jr., Glickson JD. Simultaneous measurement of arterial input function and tumor pharmacokinetics in mice by dynamic contrast enhanced imaging: effects of transcytolemmal water exchange. Magn Reson Med 2004; 52:248–257.

27. Li X, Welch EB, Chakravarthy AB, et al. Statistical comparison of dynamic contrast-enhanced MRI pharmacokinetic models in human breast cancer. Magn Reson Med 2012;68:261–271.

28. Yankeelov TE, Gore JC. Dynamic contrast enhanced magnetic resonance imaging in oncology: theory, data acquisition, analysis, and examples. Curr Med Imaging Rev 2009;3:91–107.

29. Li X, Welch EB, Chakravarthy AB, et al. A novel AIF detection method and a comparison of DCE-MRI parameters using individual and population based AIFs in human breast cancer. Phys Med Biol 2011;56:5753–5769.

30. Lehmann EL. Parametric versus nonparametrics: two alternative methodologies. J Nonparametric Stat 2009;21:397–405.

31. Benjamini Y, Hochberg Y. Controlling the false discovery rate: a practical and powerful approach to multiple testing. J R Stat Soc 1995;57: 289–300.

32. Robin X, Turck N, Hainard A, Tiberti N, Lisacek F, Sanchez JC, Muller M. pROC: an open-source package for R and S+ to analyze and compare ROC curves. BMC Bioinformatics 2011;12:77.

33. Perkins NJ, Schisterman EF. The inconsistency of "optimal" cut-points obtained using two criteria based on the receiver operating characteristic curve. Am J Epidemiol 2006;163:670–675.

34. R Development Core Team. R: A language and environment for statistical computing. Foundation for Statistical Computing, Vienna, Austria 2008 ISBN 3-900051-07-0.

35. Pickles MD, Lowry M, Manton DJ, Gibbs P, Turnbull LW. Role of dynamic contrast enhanced MRI in monitoring early response of locally advanced breast cancer to neoadjuvant chemotherapy. Breast Cancer Res Treat 2005;91:1–10.

36. Macura KJ, Ouwerkerk R, Jacobs MA, Bluemke DA. Patterns of enhancement on breast MR images: interpretation and imaging pitfalls. Radiographics 2006;26:1719–1734; quiz 1719.

37. Wedam SB, Low JA, Yang SX, et al. Antiangiogenic and antitumor effects of bevacizumab in patients with inflammatory and locally advanced breast cancer. J Clin Oncol 2006;24:769–777.

38. Li SP, Taylor NJ, Makris A, Ah-See ML, Beresford MJ, Stirling JJ, d'Arcy JA, Collins DJ, Padhani AR. Primary human breast adenocarcinoma: imaging and histologic correlates of intrinsic susceptibility-weighted MR imaging before and during chemotherapy. Radiology 2010;257:643–652.

39. Hylton NM, Blume JD, Bernreuter WK, et al. Locally advanced breast cancer: MR imaging for prediction of response to neoadjuvant chemotherapy-results from ACRIN 6657/I-SPY TRIAL. Radiology 2012;263:663–672.

40. Hylton NM. Vascularity assessment of breast lesions with gadolinium-enhanced MR imaging. Magn Reson Imaging Clin N Am 1999;7: 411–420, x.

41. Li X, Dawant BM, Welch EB, et al. A nonrigid registration algorithm for longitudinal breast MR images and the analysis of breast tumor response. Magn Reson Imaging 2009;27:1258–1270.

42. Li X, Dawant BM, Welch EB, et al. Validation of an algorithm for the nonrigid registration of longitudinal breast MR images using realistic phantoms. Med Phys 2010;37:2541–2552.

43. Henderson E, Rutt BK, Lee TY. Temporal sampling requirements for the tracer kinetics modeling of breast disease. Magn Reson Imaging 1998;16:1057–1073.

44. Wang Y, Huang W, Panicek DM, Schwartz LH, Koutcher JA. Feasibility of using limited-population-based arterial input function for pharmacokinetic modeling of osteosarcoma dynamic contrast-enhanced MRI data. Magn Reson Med 2008;59:1183–1189.

45. Meng R, Chang SD, Jones EC, Goldenberg SL, Kozlowski P. Comparison between population average and experimentally measured arterial input function in predicting biopsy results in prostate cancer. Acad Radiol 2010;17:520–525.

46. Wolff AC, Berry D, Carey LA, et al. Research issues affecting preoperative systemic therapy for operable breast cancer. J Clin Oncol 2008; 26:806–813.

47. Fisher B, Bryant J, Wolmark N, et al. Effect of preoperative chemotherapy on the outcome of women with operable breast cancer. J Clin Oncol 1998;16:2672–2685.

48. Bear HD, Anderson S, Smith RE, et al. Sequential preoperative or postoperative docetaxel added to preoperative doxorubicin plus cyclophosphamide for operable breast cancer:National Surgical Adjuvant Breast and Bowel Project Protocol B-27. J Clin Oncol 2006;24: 2019–2027.

49. Loo CE, Straver ME, Rodenhuis S, Muller SH, Wesseling J, Vrancken Peeters MJ, Gilhuijs KG. Magnetic resonance imaging response monitoring of breast cancer during neoadjuvant chemotherapy: relevance of breast cancer subtype. J Clin Oncol 2011;29:660–666.

50. De Los Santos J, Bernreuter W, Keene K, Krontiras H, Carpenter J, Bland K, Cantor A, Forero A. Accuracy of breast magnetic resonance imaging in predicting pathologic response in patients treated with neoadjuvant chemotherapy. Clin Breast Cancer 2011;11:312–319.

51. Arlinghaus LR, Welch EB, Chakravarthy AB, et al. Motion correction in diffusion-weighted MRI of the breast at 3T. J Magn Reson Imaging 2011;33:1063–1070.

52. O'Connor JP, Rose CJ, Jackson A, et al. DCE-MRI biomarkers of tumour heterogeneity predict CRC liver metastasis shrinkage following bevacizumab and FOLFOX-6. Br J Cancer 2011;105:139–145.

53. Ma B, Meyer CR, Pickles MD, Chenevert TL, Bland PH, Galban CJ, Rehemtulla A, Turnbull LW, Ross BD. Voxel-by-voxel functional diffusion mapping for early evaluation of breast cancer treatment. Inf Process Med Imaging 2009;21:276–287.